Quim. Nova, Vol. 40, No. 10, 1137-1140, 2017 http://dx.doi.org/10.21577/0100-4042.20170106

Artigo

THEORETICAL RESEARCH ON THE MULTI-CHANNEL REACTION MECHANISM AND KINETICS OF HNCS WITH OH^-

Li-Jie Hou[a,*], Bo-Wan Wu[a], Yan-Xia Han[a], Chao Kong[a] and Li-Guo Gao[b]
[a]College of Chemistry & Chemical Engineering, Longdong University, 745000, Qingyang, China
[b]School of Chemistry & Chemical Engineering, Yulin University, 719000, Yulin, China

Recebido em 07/03/2017; aceito em 26/06/2017; publicado na web em 15/08/2017

We presented a theoretical study on the detailed reaction mechanism and kinetics of the HNCS molecule with the OH^-. The barrierless minimum energy path and the most favorable entrance channel have been determined by study the thermodynamic and kinetic characters of the channel with low energy barrier. The B3LYP/6-311++G** method was employed for all the geometrical optimizations and a multi-level extrapolation method based on the G3 energies was employed for further energy refinements. In addition, the analysis of the combining interaction between hydroxide ion and HNCS was performed by natural bond orbitals (NBO) analysis. The calculation results indicated that the reaction of OH^- with HNCS had four channels, and the channel of H-atom in HNCS direct extraction to OH^- (OH^-+HNCS→IM1→TS3→IM4→P2(SCN^- +H_2O)) in singlet state was the main channel with the low potential energy and high equilibrium constant and reaction rate constant. SCN^- and H_2O were main products.

Keywords: hydroxide ion; isothiocyanic acid; mechanism; equilibrium constant

INTRODUCTION

The problem of the severe air pollution in developing countries has caused wide public concern over the recent years, heavy power plant smoke and car emissions, mainly in the form of sulfate, organic, nitric acid and particles, have always been a threat to the global public health. In the meanwhile, as important intermediates of sulfur-containing fuel combustion process, HNCS and its derived free radical NCS can participate in the process of removal the toxic NO_4 compounds from rapid combustion exhaust gas too.[1-6] Due to its important role, the theoretical study on the reaction mechanism of HNCS with small molecules by quantum chemistry calculation also become the focus of the chemical workers' research.[7-19]

Because its oxidation ability is very strong, hydroxide ion (OH^-) is one of the key intermediates in the interstellar environment and a large number of combustion reaction, not only represents a very important role that OH^- can oxidized volatile organic compounds in the troposphere gas,[20] but also plays an important role in atmospheric chemistry where it is the primary process responsible for removal of the H_2CO pollutant.[21-25] Molecular anions play an important role in the chemistry of the interstellar medium, of carbon stars , and the Earth' s ionosphere. One such species is the hydroxide ion. Madura and Jorgensen applied ab initio calculation to discuss the addition of hydroxyl anion to the aldehydic carbon atom.[26] Herein, we used the density functional theory (DFT) to explore the reaction mechanism of OH^- with HNCS, We hope our work might provide theoretical guidance to control NO_x substance-related air pollution effectively.

CALCULATION METHODS

All calculations were performed with the Gaussian 03 package.[27] The geometries of reactants, intermediates, transition states and products were optimized at the DFT-B3LYP/6-311++G** level.[28-31] The harmonic vibration frequencies obtained at the corresponding level were used to characterize the stationary points and first-order saddle points. The intrinsic reaction coordinate (IRC) calculation was used to track minimum energy paths from transition structures to stationary points. To obtain more precise energy results, stationary point energies were calculated at the G3 level. The thermodynamic and kinetic characters of the channel with low energy barrier were calculated by the statistical thermodynamics and Eyring transition state theory with Winger correction at different temperatures.

*e-mail: 200hlj@163.com

RESULTS AND DISCUSSION

Channels of singlet state OH^- with HNCS

Calculations showed the reaction of singlet state OH^- with HNCS had four channels. NBO calculation results indicated that precursor complex IM1 formed when the lone electron pair of O-atom in OH^- interacted with σ^*(C–S) and σ^*(N–H) in HNCS, respectively.[32] The abstraction reactions of S-atom and H-atom in HNCS transfer occurred by using IM1 as starting intermediate. The lone electron pair of O-atom in OH^- and N-atom in HNCS interacted with the σ^*(C–S) and σ^*(C–N) of HNCS to form IM1 intermediate. This interaction leaded to the reduction of O–C and N–H bond strength, and prompted H-atom in OH^- transfer. Therefore, the reaction of singlet state OH^- with HNCS was complicated and multichannel.

H1-atom in HNCS transfer to OH^- channel

HNCS collided with the singlet state OH^- to form an intermediate IM1, and then IM1 generated intermediate IM4 via transition state TS3. After that, IM4 dissociated to generate product P2 (SCN+H_2O). As shown in Figure 1, the bond length of H1–N in HNCS increased from IM1 (0.1022 nm) to TS3 (0.1207 nm) to IM4 (0.2078 nm) and the bond length of H1–O was gradually decreased from 0.2062 nm (IM1) to 0.1223 nm (TS3). This result indicated that H1–N bond cleaved and H1–O bond formed gradually in this process. The H-atom of HNCO directly bonded with O-atom in OH^-, and the reaction of H1-atom in HNCS transfer to OH^- performed. As shown in Figure 2, the energy barrier of the reaction step from IM1 to IM4 via TS3 was 285.3 kJ mol^{-1}, which was lower and advantageous in kinetics. The whole reaction was exothermic, and the heat generated in reaction was 616.0 kJ mol^{-1}, which was thermodynamically favorable to

this reaction process. As could be see from Table 1, the rate and equilibrium constants of reaction were large at the temperature range of 700 to 2000 K. Therefore, the channel of H1-atom in HNCS transfer to OH^- was the major reaction channel.

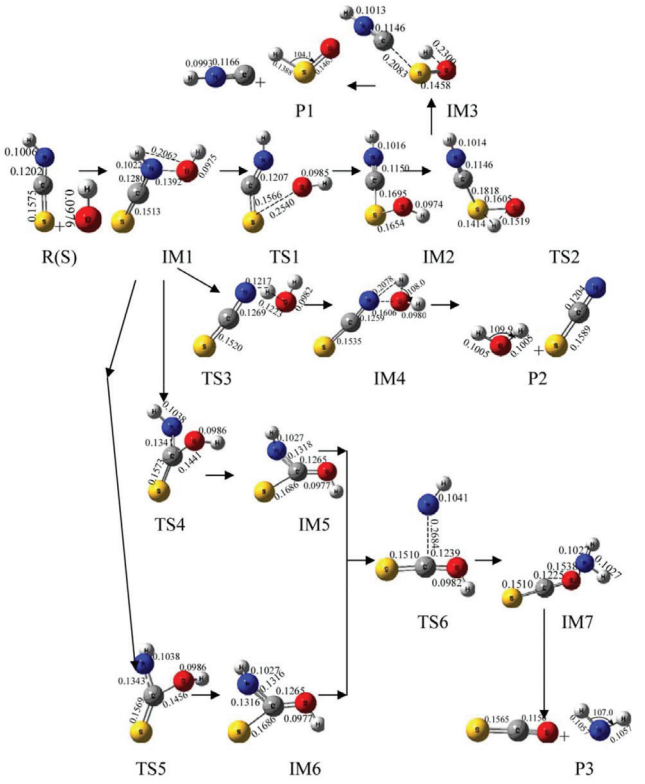

Figure 1. *Optimized geometries of various species in reaction in singlet state (bond lengths in nm and bond angles in degree)*

S-atom abstraction channel

In Figure 1, the S atom combined with O atom of IM1 to form a stable intermediate IM2 through transition state TS1. In IM2, σ (C–S) interacted with σ* (C–N) and the lone electrons pairs of S-atom and N-atom in HNCS, leading to the weakening of C–S bond. From IM1 to IM2, the C–S bond length increased to 0.1566 from 0.1513 nm, the O–S bond length decreased to 0.1654 nm in IM2 from 0.2540 nm in TS1, which indicated that the strength of C–S bond gradually weakened and the strength of O–S bond gradually enhanced. Subsequently, IM2 generated IM3 through transition state TS2, and then IM3 dissociated to generate product P1 (HSO^-+CNH), and S-atom abstraction was completed. The energy barrier was 340.4 kJ mol^{-1} from IM1 to IM2, and that of the reaction step from IM3 to IM2 was 317.3 kJ mol^{-1}. The whole reaction was exothermic reaction with 518.3 kJ mol^{-1} of heat liberated. Moreover, the reaction equilibrium and rate constants were small in the temperature range from 100 to 1600 K. Therefore, this reaction process was a minor reaction channel.

H2-atom in OH^- transfer to NH channel

IM1 through TS4 and TS5 form intermediate IM5 and IM6 with the reaction energy barrier of 271.3 and 223.2 kJ mol-1 respectively. In this step, the length of C–O bond changed from 0.1441nm in TS4 and 0.1456 nm in TS5 to 0.0977 nm in IM6(Figure 1)which indicated that C–O bond gradually enhanced until their formation. It is worth mentioning that IM5 and IM6 is cis-trans isomer. From IM5 and IM6 to TS6, the lengths of C–N bond increased to 0.2684 nm from 0.1265 nm. These results indicated that N–C bond gradually

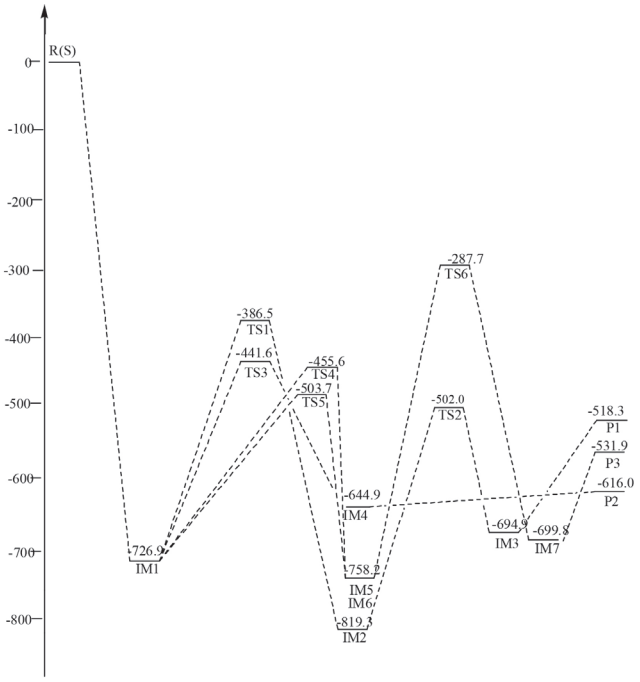

Figure 2. *Schematic map of energy levels in singlet state (relative energies in kJ mol^{-1})*

weakened and fracture until IM7 generated in this reaction process. Afterwards, IM7 dissociated to product P3(NH_2^-+COS). The whole reaction was exothermic with the total liberated heat of 531.9 kJ mol^{-1}, and the energy barrier from IM5 and IM6 to IM7 through TS6 was 470.5 kJ mol^{-1} which was higher than that of the major reaction channel. The reaction rate constants of H2-atom in OH^- transfer to NH channel was large, but the equilibrium constants were small at the temperature range from 100 to 1200 K. Therefore, these two channels were not the major reaction pathway.

Channels of triplet state OH^- with HNCS

Calculation results indicated that triplet state OH^- could also react with HNCS. This reaction had two channels including absorption of $^3OH^-$ and H1-atom in HNCS transfer to OH^- channel. The NBO results showed the lone electron pair of O-atom in ^3OH anions interacted with σ*(C–N) of HNCS in $^3IM1$ which was used as the precursor complex to accomplish absorption OH^- reaction. $^3IM2$ formed due to the interaction between σ*(N–H) of HNCS with the lone electron pair of O-atom in ^3OH, which leaded to the weakening of N–H bond and the occurring of H1-atom transfer to OH^- reaction.

OH^- abstraction channel

The lone electron pair of O-atom in $^3OH^-$ interacted with σ*(C–N) of HNCS to form $^3IM1$, which could generated product $^3P1$($^3HNCSOH^-$) through $^3TS1$. As shown in Figure 3, the length of C–O bond decreased to 0.1300 nm ($^3IM1$) from 0.1210 nm ($^3P1$). In this process, the strength of C–O bond formed gradually. Finally, OH^- combined with C, and the direct extraction OH^- reaction was accomplished. As shown in Figure 4, the energy barrier was 144.8 kJ mol^{-1} in the reaction step from $^3IM1$ to $^3P1$ through $^3TS1$. The whole reaction released 446.3 kJ mol^{-1}.

H1-atom in HNCS transfer to OH^- channel

In Figure 4, $^3IM2$ formed $^3IM3$ through transition state $^3TS2$ with the energy barrier of 308.5 kJ mol^{-1}, and the length of H1–N bond increased to 0.1257 nm ($^3TS2$) from 0.1532 nm ($^3IM2$). The length

Table 1. In temperature range of from 100 to2000 K, the equilibrium constant (K) and rate constant (k(s)) of the reaction in singlet state with low energy barrier at 1.0 atm

T/K	IM1→P1	IM1→P2	IM1→P3	IM1→TS3→IM4	IM1→TS4→IM5	IM1→TS5→IM5	IM5→TS6→IM7	IM6→TS6→IM7
	K	K	K	k/s^{-1}	k/s^{-1}	k/s^{-1}	k/s^{-1}	k/s^{-1}
100	3.92×10^{-132}	8.68×10^{131}	5.68×10^{341}	4.30×10^{-87}	2.30×10^{-92}	4.65×10^{-101}	6.49×10^{-204}	6.41×10^{-204}
200	3.89×10^{-63}	1.78×10^{62}	8.57×10^{240}	3.09×10^{-37}	3.11×10^{-40}	1.40×10^{-44}	3.21×10^{-95}	3.19×10^{-95}
300	5.56×10^{-40}	1.61×10^{39}	1.23×10^{163}	1.21×10^{-20}	7.56×10^{-23}	9.56×10^{-26}	1.02×10^{-58}	1.01×10^{-58}
400	2.28×10^{-28}	5.46×10^{28}	1.59×10^{124}	2.44×10^{-12}	3.90×10^{-14}	2.63×10^{-16}	2.32×10^{-40}	2.31×10^{-40}
500	2.14×10^{-21}	4.70×10^{21}	7.44×10^{100}	2.42×10^{-7}	6.86×10^{-9}	1.26×10^{-10}	2.68×10^{-29}	2.67×10^{-29}
600	9.44×10^{-17}	1.99×10^{16}	2.06×10^{85}	5.31×10^{-4}	2.21×10^{-5}	7.95×10^{-7}	6.72×10^{-22}	6.69×10^{-22}
700	1.93×10^{-13}	3.99×10^{13}	1.56×10^{74}	0.13	7.23×10^{-3}	4.20×10^{-4}	1.34×10^{-16}	1.33×10^{-16}
800	5.79×10^{-11}	1.18×10^{10}	6.96×10^{65}	8.45	0.56	4.69×10^{-2}	1.28×10^{-12}	1.28×10^{-12}
900	4.81×10^{-9}	9.81×10^{9}	2.20×10^{59}	217.07	16.81	1.86	1.62×10^{-9}	1.61×10^{-9}
1000	1.63×10^{-7}	3.33×10^{7}	1.36×10^{54}	2.95×10^{3}	256.29	35.40	4.95×10^{-7}	4.93×10^{-7}
1200	3.12×10^{-5}	6.41×10^{5}	2.03×10^{46}	1.50×10^{5}	1.54×10^{4}	2.99×10^{3}	2.67×10^{-3}	2.66×10^{-3}
1400	1.28×10^{-3}	2.67×10^{3}	5.00×10^{40}	2.54×10^{6}	2.91×10^{5}	7.17×10^{4}	1.25	1.25
1600	2.03×10^{-2}	4.27×10^{2}	3.02×10^{36}	2.14×10^{7}	2.65×10^{6}	7.83×10^{5}	126.54	126.09×10^{3}
1800	0.17	872.9	1.54×10^{33}	1.14×10^{8}	1.48×10^{7}	5.05×10^{6}	5.05×10^{3}	4.59×10^{3}
2000	0.92	0.36	3.51×10^{30}	4.33×10^{8}	5.90×10^{7}	2.25×10^{7}	8.195×10^{4}	8.16×10^{4}

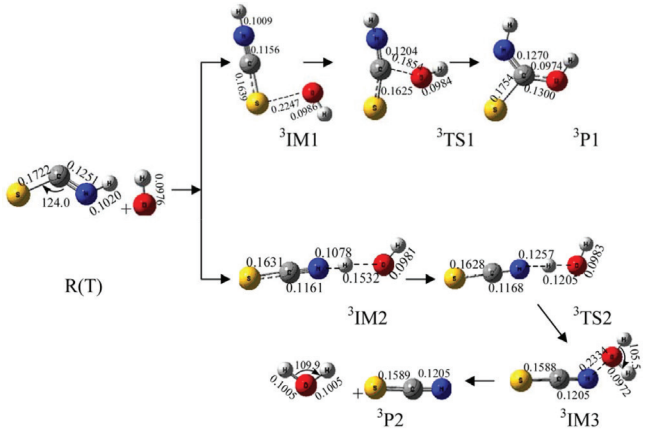

Figure 3. *Optimized geometries of various species in reaction in triplet state (bond lengths in nm and bond angles in degree)*

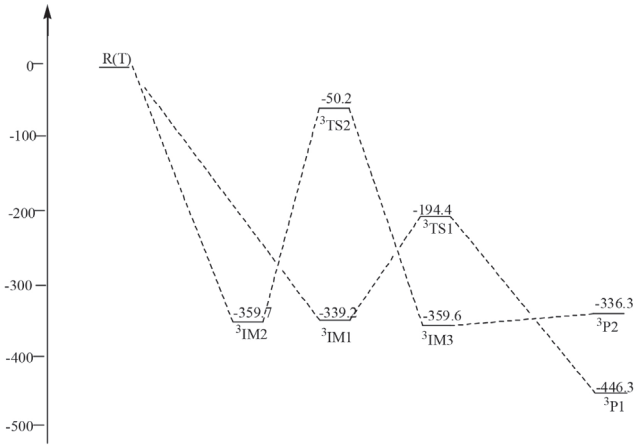

Figure 4. *Schematic map of energy levels in triplet state (relative energies in kJ mol^{-1})*

of H1–O bond varied from 0.1532 nm (^{3}IM2) to 0.1185 nm (^{3}TS2) to 0.0972 nm (^{3}IM3). In this step, H1–O bond formed and H1–N bond dissociated gradually. The formation of ^{3}IM3 from ^{3}IM2 through transition state ^{3}TS2 had the energy barrier of 309.5 kJ mol^{-1}. Finally, ^{3}IM3 dissociated into generate product ^{3}P2 ($^3SCN^-+H_2O$).

Comparing the two pathways, the direct extraction OH^- channel had the lowest energy barrier. Therefore, the direct extraction OH^- channel was the major reaction channel in the reaction of triplet state OH^- with HNCS.

CONCLUSIONS

In this study, the B3LYP method of density functional theory was employed to research the reaction mechanism of OH^- and HNCS. The calculation results showed that the reaction of singlet state had four feasible pathways and that of triplet state was two. The H1-atom in HNCS transfer to OH^- channel in singlet state reaction was the main reaction channel with the lowest energy barrier. The rate constant and equilibrium constant of the H1-atom in HNCS transfer to OH^- channel in singlet state were higher than other channels in the temperature range of 100 to 2000 K. This study might provide theoretical clue to control environment pollution. By comparing with the main channel of singlet state reaction, the energy barrier of this pathway was higher. So, the reaction of triplet state was not the predominant way of OH^- with HNCS reaction.

SUPPLEMENTARY MATERIAL

A table with the energies, relative energies and frequencies of the reaction can be found at http://quimicanova.sbq.org.br in pdf format, with free access.

ACKNOWLEDGMENTS

This work was supported by the Scientific Research Project of Gansu Province Higher Education (No.2016B-098) and the Applied Chemistry Key Subject of Gansu Province (No. GSACKS20130113) .

REFERENCES

1. Northrup, F. J.; Sears T. J.; *Chem. Phys. Lett.* **1989**, *159*, 421.
2. Baren, R. E.; Hershberger, J. F.; *J. Phys. Chem. A* **1999**, *103*, 11340.
3. Perry, R. A.; Siebers, D. L.; *Nature* **1986**, *324*, 657.
4. Miller, J. A.; Bowman, C. T.; *Prog. Energy Combust. Sci.* **1989**, *15*, 287.
5. Miller, J. A.; Bowman, C. T.; *Int. J. Chem. Kinet.* **1991**, *23*, 289.
6. Brown, S. S.; Berghot, H. L.; Crim, F. F.; *J. Phys. Chem. A* **1996,** *100*, 7948.
7. McDonald, J. R.; Scherr, V. M.; McGlynn, S. P.; *J. Chem. Phys.* **1969**, *51*, 1723.
8. Wierzejewska, M.; Wieczorek, R.; *J. Chem. Phys.* **2003,** *287*, 169.
9. Wierzejewska, M.; Olbert-Majkut, A.; *J. Phys. Chem. A.* **2003**, *107*, 1928.
10. Hou, L. J.; Kong, C.; Han, Y. X.; Chen, D. P.; Gao, L. G.; *J. At. Mol. Phys.* **2012**, *29*, 988.
11. Kong, C.; Han, Y. X.; Chen, D. P.; *J. At. Mol. Phys.* **2011**, *28*, 823.
12. Hou, L. J.; Kong, C.; Han, Y. X.; Chen, D. P.; Gao, L. G.; *J. At. Mol. Phys.* **2013**, *30*, 707.
13. Li-Jie, H.; Bo-Wan, W.; Yan-Xia, H.; *Comput. Theor. Chem.* **2015**, *1051*, 57.
14. Liu, P. J.; Zhao, M.; Pan, X. M.; *Acta Chim. Sin.* **2004**, *62*, 1991.
15. Liu, P. J.; Du, Q. S.; Chang, Y. F.; *Acta Phys.-Chim. Sin.* **2005**, *12*, 1347.
16. Liu, P. J.; Zhang, L. H.; Sun, H.; Chang, Y. F.; Wang, R. S.; *Chem. Res. Chin. Univ.* **2006**, *22*, 635.
17. Xu, B. H.; Li, L. C.; Zhu, Y. Q.; *Acta Sci. Nat. Univ. Szechuan.* **2007**, *44*, 653.
18. Han, Y. X.; Gang, Z. Y.; Wang, Y. C.; Liang, J. X.; Yan, P. J.; *Acta Chim. Sin.* **2009**, *67*, 773.
19. Cuihong, S.; Ying, L.; Baoen, X.; Zeng, Y.; Meng, L.; Zhang, S.; *J. Chem. Phys.* **2013**, *139*, 154307-1.
20. Wayne, R. P.; Chemistry of Atmospheres, 2nd ed., Clarendon Press: Oxford, 1991.
21. Anglada, J. M.; *J. Phys. Chem. A* **2005**, *109*, 10786.
22. Alvarez-Idaboy, J. R.; Mora-Diez, N.; Boyd, R. J.; Vivier-Bunge, A.; *J. Am. Chem. Soc.* **2001**, *123*, 2018.
23. Aloisio, S.; Francisco, J. S.; *J. Phys. Chem. A* **2000**, *104*, 3211.
24. Takahashi, H.; Hori, T.; Wakabayashi, T.; Nitta, T.; *J. Phys. Chem. A* **2001**, *105*, 4351.
25. Li, H.-Y.; Pu, M.; Ji, Y.-Q.; Xu, Z.-F.; Feng, W.-L.; *J. Chem. Phys.* **2004**, *307*, 35.
26. Madura, J. D; Jorgensen, W. L.; *J .Am .Chem .Soc.* **1986**, *108*, 2517.
27. Frisch, M. J.; Trucks, G. W.; Schlegel, H. B.; Scuseria, G. E.; Robb, M. A.; Cheeseman, J. R.; Montgomery, Jr., J. A.; Vreven, T.; Kudin, K. N.; Burant, J. C.; Millam, J. M.; Iyengar, S. S.; Tomasi, J.; Barone, V.; Mennucci, B.; Cossi, M.; Scalmani, G.; Rega, N.; Petersson, G. A.; Nakatsuji, H.; Hada, M.; Ehara, M.; Toyota, K.; Fukuda, R.; Hasegawa, J.; Ishida, M.; Nakajima, T.; Honda, Y.; Kitao, O.; Nakai, H.; Klene, M.; Li, X.; Knox, J. E.; Hratchian, H. P.; Cross, J. B.; Bakken, V.; Adamo, C.; Jaramillo, J.; Gomperts, R.; Stratmann, R. E.; Yazyev, O.; Austin, A. J.; Cammi, R.; Pomelli, C.; Ochterski, J. W.; Ayala, P. Y.; Morokuma, K.; Voth, G. A.; Salvador, P.; Dannenberg, J. J.; Zakrzewski, V. G.; Dapprich, S.; Daniels, A. D.; Strain, M. C.; Farkas, O.; Malick, D. K.; Rabuck, A. D.; Raghavachari, K.; Foresman, J. B.; Ortiz, J. V.; Cui, Q.; Baboul, A. G.; Clifford, S.; Cioslowski, J.; Stefanov, B. B.; Liu, G.; Liashenko, A.; Piskorz, P.; Komaromi, I.; Martin, R. L.; Fox, D. J.; Keith, T.; Al-Laham, M. A.; Peng, C. Y.; Nanayakkara, A.; Challacombe, M.; Gill, P. M. W.; Johnson, B.; Chen, W.; Wong, M. W.; Gonzalez, C.; Pople, J. A.; *Gaussian 03, Revision B.01*, Gaussian, Inc., Wallingford CT, 2004.
28. Su, M. D.; Chu, S. Y.; *J. Am. Chem. Soc.* **1999**, *121*, 4229.
29. Becke, A. D.; Kohn, W.; Parr, R. G.; *J. Phys. Chem.* **1996**, *100*, 12974.
30. Becke, A. D.; *Phys. Rev. A* **1988**, *38*, 3098.
31. Fukui, K. A.; *J. Phys. Chem.* **1970**, *74*, 4161.
32. Reed, A. E.; Curtiss, L. A.; Weinhold, F.; *Chem. Rev.* **1988**, *88*, 899.